Hindawi Publishing Corporation
Advances in Materials Science and Engineering
Volume 2013, Article ID 692635, 11 pages
http://dx.doi.org/10.1155/2013/692635

Research Article

Fibre Laser Cutting and Chemical Etching of AZ31 for Manufacturing Biodegradable Stents

Ali Gökhan Demir,[1] Barbara Previtali,[1] and Carlo Alberto Biffi[2]

[1] *Department of Mechanical Engineering, Politecnico di Milano, Via La Masa 1, 20156 Milan, Italy*
[2] *National Research Council, Institute for Energetics and Interphases, Corso Promessi Sposi 29, 23900 Lecco, Italy*

Correspondence should be addressed to Ali Gökhan Demir; aligokhan.demir@polimi.it

Received 1 May 2013; Accepted 30 July 2013

Academic Editor: Gomaa El-Damrawi

The use of magnesium-alloy stents shows promise as a less intrusive solution for the treatment of cardiovascular pathologies as a result of the high biocompatibility of the material and its intrinsic dissolution in body fluids. However, in addition to requiring innovative solutions in material choice and design, these stents also require a greater understanding of the manufacturing process to achieve the desired quality with improved productivity. The present study demonstrates the manufacturing steps for the realisation of biodegradable stents in AZ31 magnesium alloy. These steps include laser microcutting with a Q-switched fibre laser for the generation of the stent mesh and subsequent chemical etching for the cleaning of kerf and surface finish. Specifically, for the laser microcutting step, inert and reactive gas cutting conditions were compared. The effect of chemical etching on the reduction in material thickness, as well as on spatter removal, was also evaluated. Prototype stents were produced, and the material composition and surface quality were characterised. The potentialities of combining nanosecond laser microcutting and chemical etching are shown and discussed.

1. Introduction

As materials processing technology advances, advanced medical devices that depend on intrinsic material properties for their function have become available. The idea of using biocompatible and even biodegradable materials for biomedical implants has been a matter of historical discussion. The first use of Mg in a medical device, in the form of wire ligatures to stop bleeding in patients, was recorded as early as 1878 [1]. The development of high-precision micromachining technologies has enabled the use of advanced materials, realising a high precision in complex forms and small dimensions.

Biodegradability, referring to the dissolution of the medical device inside the human body once it fulfils its duty, has become one of the most attractive properties in cardiovascular stents. This property is crucial for the treatment of infant patients, because, the vessel grows as the patient grows older. Magnesium is both biocompatible and biodegradable and, as a metal, possesses mechanical properties that are superior to those of biodegradable polymers, both in terms of yield stress and maintaining the expanded shape without excessive recoil. As a result, Mg and its alloys have been receiving increased attention from the medical communities for various biomedical implant applications [2], including cardiovascular stents [3–6].

With an increasing demand in the market for stents, developing process cycles capable of maintaining high level of quality and increased productivity becomes essential. While various methods for stent manufacturing are available (such as braiding and knitting of wires, vapour deposition of the stent mesh, photochemical etching of sheets and tubes, water jet cutting of tubes, and electric discharge machining), the vast majority of the stents is produced via laser microcutting of hollow tubes [7–9]. Among these options, industrial solutions are being adapted for the laser microcutting of Mg stents, although limited information regarding the manufacturing conditions has been disclosed [5, 6, 10, 11]. On the other hand, photo-chemical machining has been demonstrated to be a suitable production method for magnesium-alloy stents [12, 13]. As the most commonly applied process in industrial

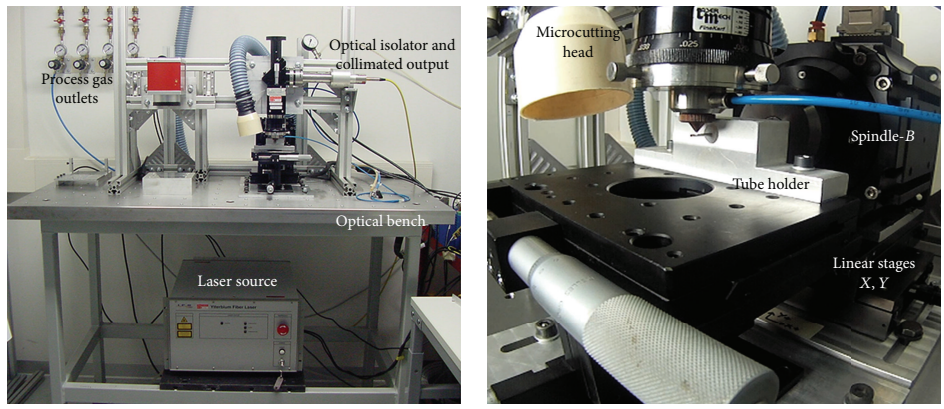

(a) (b)

Figure 1: Laser microcutting setup used for the laser microcutting of AZ31 tubes.

stent production, laser microcutting provides a flexible solution for achieving complex geometries on a variety of materials without requiring the use of dedicated masks or dies. In the last decade, the introduction and rapid diffusion of fibre lasers into the market have resulted in their utilisation in microcutting applications that includes stent fabrication [14–16]. Ultra-fast lasers with ps to fs pulse durations have been applied to stent fabrication, providing improved cutting quality with limited thermal damage on the material [17–19]. These systems still require higher capital and maintenance costs than other laser systems. A balance between quality and productivity is essential, first to fulfil the market demand and subsequently to reduce production costs. This balance can be achieved by combining laser microcutting process characterised by a good balance between productivity and low thermal damage (as would be provided by ns-pulse lasers) and chemical cleaning processes and optimizing the overall process chain.

Laser processing of magnesium and its alloys has been explored sparingly. Literature dealing with the laser processing of magnesium alloys can be found mainly in the field of welding [20–22], and limited information is available in the case of laser cutting [23–25]. The existing studies describe laser cutting in the macrodimensional range, whereas limited information is available on the microcutting of these alloys [26]. Although biodegradable stents in Mg alloys are currently being developed industrially, with ongoing clinical trials, to authors' knowledge, there is no literature dealing with the manufacturing of these devices.

This study describes the manufacturing of biodegradable Mg stents in AZ31 alloy. The production cycle involves laser microcutting of small diameter tubes with a Q-switched fibre laser operating in ns-pulse regime, followed by a finishing operation of chemical etching with an HNO_3 ethanol solution. The morphological and material-related attributes of the manufactured stents were characterised extensively after each production step. The results imply that the production cycle employed in this work is suitable for manufacturing the complex shape of the stent mesh on AZ31 magnesium-alloy tubes with a high precision.

2. Experimental

In this section, the novel mesh design and material selection criteria are introduced. The manufacturing steps are then presented in sequential order: first, the incision of the stent mesh on tubular material, second, chemical etching as a finishing operation for cleaning the dross and oxidised zones around the cutting area and completing the material separation. Finally, methods for evaluating kerf quality and material composition are described.

2.1. Mesh Design and Material Selection. The mesh design development is not investigated in this work. The developed mesh resulted from design optimisation through a 2D morphing procedure to retain minimum strain with maximum mass [31]. Among a group of candidate magnesium alloys, AZ31 was found to be the most suitable, due to the higher availability of the alloying elements (i.e., the alloy does not include rare earth elements). Moreover, the formability of the alloy for extrusion of semi-finished hollow tubes was found to be better [32]. The AZ31 tubes used in stent fabrication were 2.5 mm in outer diameter and 0.2 mm in thickness.

2.2. Laser Microcutting. Laser microcutting was carried out using a Q-switched fibre laser system operating in the ns-pulse regime (IPG Photonics YLP-1/100/50/50). The laser was coupled to a microcutting head with a 60 mm focal lens and a coaxial nozzle with a 0.5 mm diameter for the addition of process gas (Laser Mech Fine Kerf). To control positioning, 2 linear axis stages (X- and Y-axis) and a spindle (B-axis), both using micrometric precision, were integrated (Aerotech ALS-130, ACS-150). The system was adaptable to both 2D-flat sheet and 3D-tubular cutting. To allow handling of the small tubes without deflections a tube-holding apparatus was adapted to the system. The details of the laser microcutting setup are described in Table 1, and the system components can be seen in Figure 1.

Compared to the laser microcutting of flat sheets, laser microcutting of small tubes has a narrower process parameter window, due to machining a close profile. When ns laser

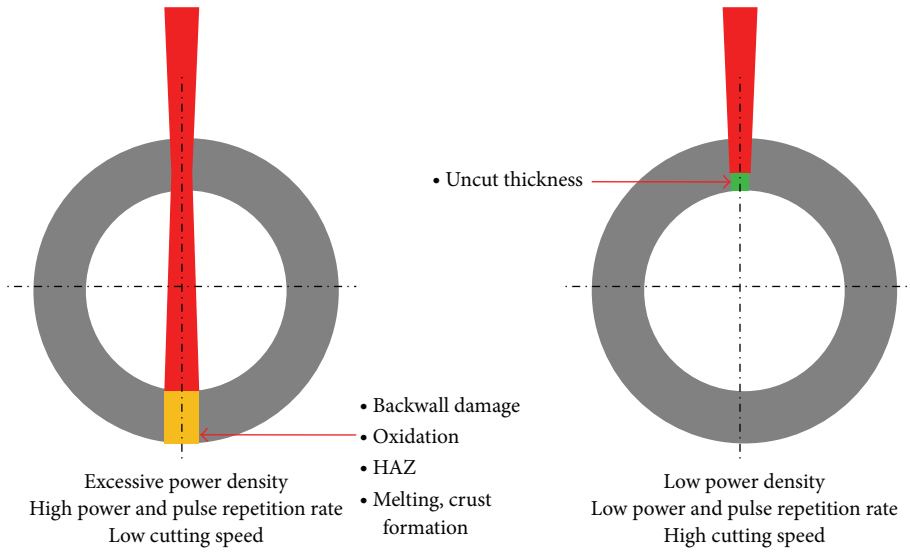

Figure 2: Common limitations in laser tube microcutting with ns-pulse laser sources.

Table 1: General specifications of the laser micromachining system used in the laser microcutting of AZ31 tubes.

IPG Photonics YLP-1/100/50/50 pulsed fibre laser	
Wavelength	1064 nm
Maximum average power	50 W
Maximum pulse energy	1 mJ
Minimum pulse duration (FWHM)	100 ns
Pulse repetition rate	20–80 kHz
Collimated beam diameter	5.9 mm
Beam quality factor (M^2)	1.7
Focused beam diameter	23 μm
High precision positioning system	
Spindle accuracy	±72.7 μrad
Linear axis accuracy	1 μm

Table 2: Processing conditions for laser microcutting of AZ31.

Average power	4.5–6.0–7.5 W
Pulse energy	0.18–0.24–0.30 mJ
Pulse repetition rate	25 kHz
Cutting speed	2 mm/s
Process gas type	Ar, O_2
Process gas pressure	7 bar
Focal position	0 mm

pulses are used, the mechanisms of material removal become a mixture of ablation from the top side of the kerf and melt expulsion from the bottom of the kerf as it is opened to its fully cut thickness. Thus, low power density conditions generate blind grooves on the material without generating a fully open kerf, while high power density conditions can machine beyond the side of the tube on which the beam is projected and cause damage to the backside (see Figure 2). Accordingly, the allowable range for the laser microcutting parameters was determined by preliminary experiments on flat AZ31 sheets with 200 μm to achieve cutting conditions suitable for generating the fine mesh geometry. Average power of the laser was varied between 4.5–7.5 W, while pulse repetition rate was fixed as 25 kHz. Cutting speed of 2 mm/s was used to allow the positioning system to operate in the correct regime within the complicated mesh trajectory. Regarding the process gas, literature pertaining to the laser cutting of Mg alloys describes the issues of dross formation and related limitations in the quality of the cut kerf. One proposed method for dealing with these issues involves the use of multiple assist gas nozzles and the manipulation of the gas flow to facilitate the movement of molten material [23]. Due to dimensional restrictions, these considerations were not applicable in this study. Instead, two different process gas conditions for microcutting were studied: an inert gas condition using Ar (purity 99.998%) and a reactive-cutting condition using O_2 (purity 99.95%) in which the oxidation enthalpy is combined with the laser energy. Both conditions were applied at a pressure of 7 bar. This intermediate value was chosen, because higher pressures can cause material deflection throughout the laser microcutting operation. Although lower pressures can be preferable for reactive gas cutting involving O_2, in this case, an intermediate pressure was chosen to include the mechanical ejection of material from the bottom of the opened kerf. The laser microcutting conditions are summarised in Table 2. Chemical etching was employed on the stent mesh cut on flat sheets until separation was achieved or 25% of the material thickness was lost. The conditions were compared in terms of full separation after chemical etching, and parameter sets were determined for tube cutting.

On the tubular material, first, linear incisions were made along the tube axis to characterise the kerf quality after laser microcutting and chemical etching. The same conditions were used for the laser microcutting of the stent mesh on the tubes.

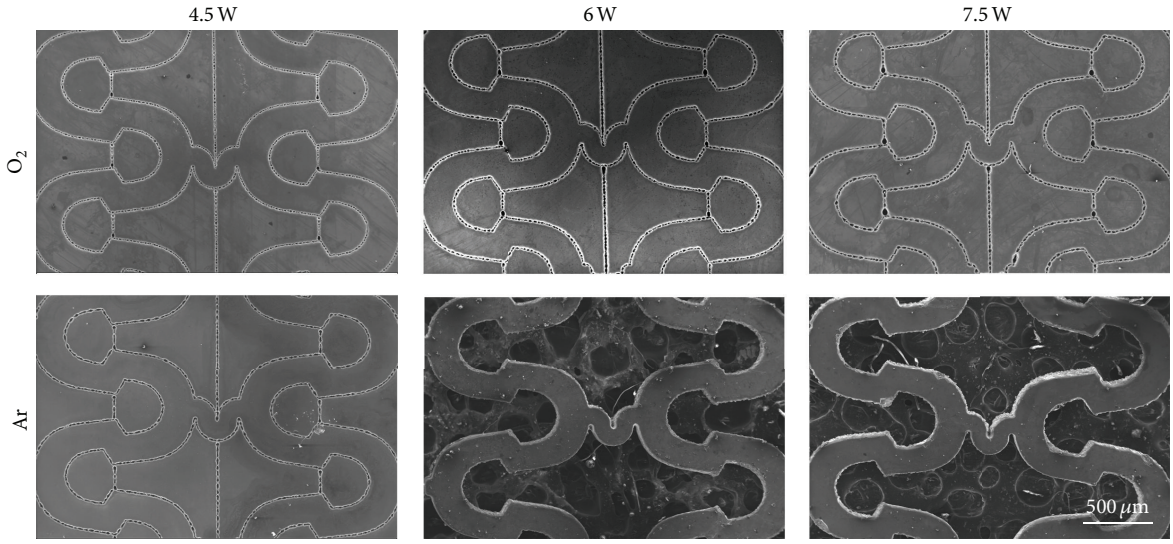

Figure 3: Laser cutting of stent mesh with different power and process gas conditions on flat AZ31. Samples show results after chemical etching. The non-separated specimens were etched until the sheet thickness was reduced to 0.16 mm.

2.3. Chemical Etching. A solution consisting of 10 mL HNO_3 and 90 mL ethanol was employed, based on an etchant used for magnesium polishing [33]. Chemical etching was applied at room temperature, and after immersion in the etching solution, the samples were rinsed with water, cleaned in an ultrasonic bath, while being submerged in ethanol, and then dried in ambient air. Each set of samples was etched in 50 mL of fresh etchant. Although the etching step is intended to remove the dross and recast areas around the cutting zone, it is possible that the solution may also significantly etch the stent body, causing a reduction in both weight and thickness [34]. Thus, the effect of the etching solution in reducing the thickness of the material was first studied on 0.4 mm thick AZ31 flat sheets. When samples were immersed for less than 5 seconds, etching did not activate, no cleaning effect was observed, and no significant thickness reduction was measured. The etching duration was thus varied between 5–600 seconds. Specimens were photographed before and after chemical etching using an optical microscope (Leitz Ergolux 200), and the thicknesses were measured using image processing software (Leica IM50). Using these measurements, a regression model was derived to predict the thickness reduction (Δr [μm]) as a function of etching time (t [s]) for etching durations ranging between 5–600 seconds. This model was used to determine the limiting etching duration that would generate a 20 μm thickness reduction, which corresponds to 10% of the tube thickness used for stent manufacturing. Chemical etching was then applied to the laser microcut stents, for this determined duration to reveal the efficacy of the process in removing the dross and completing the kerf separation.

2.4. Methods and Instruments for the Evaluation of Kerf Quality. Scanning electron microscopy (SEM) was applied to capture morphological images of the linear cuts after the laser microcutting and chemical etching steps to assess their geometrical attributes (Zeiss LEO 1430). Spatter height was also measured from the SEM images, with 4 replications taken along the cutting axis. The incisions on the tubes were sectioned after chemical etching to reveal the kerf geometry. The kerf width was measured at the laser entrance and exit sides on the transverse sections of the cuts, with 4 replications. SEM images were also obtained for the laser microcut stents after each processing step for qualitative morphological analysis.

The chemical composition of the final stent produced with the chosen processing conditions was also characterised. Energy-dispersive X-ray spectroscopy (EDS) was used to identify material chemical composition after each manufacturing step, which was compared to the initial composition. Three measurements were taken at two distinct positions, as follows.

(i) The stent wall: the side of the laser-microcut kerf that remains on the stent body.

(ii) The external surface of the stent: the part of stent that does not interact directly with the laser beam, which is the contour defined by the outer diameter of the tubular raw material.

Imaging with back scattered electrons was also employed to reveal differences in elemental mass and thereby revealing the oxidation zones. Surface roughness measurements were carried out on the stent wall with focus-variation-based optical imaging (Alicona Infinite Focus).

3. Results

3.1. Laser Microcutting. The initial cuts made on the flat sheets revealed the strong influence of the process gas, as complete separation after chemical etching was only possible in the case of cuts made with Ar (see Figure 3). In this case the minimum average power level for complete separation

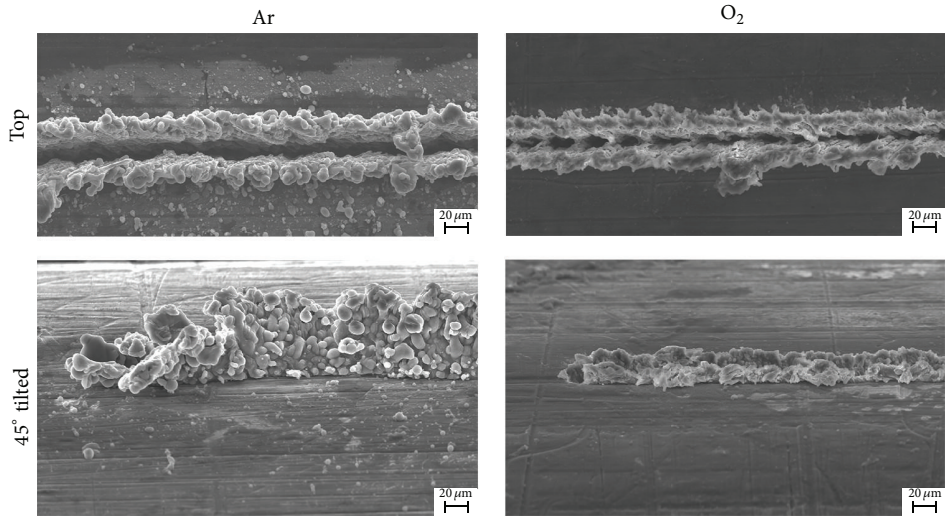

Figure 4: SEM images of the linear incisions on the AZ31 tube obtained with Ar and O_2 process gasses.

after chemical etching was 6 W. The stent meshes cut with O_2 were not separable from the scrap in any of the experimented conditions, and the chemical etching was stopped when the thickness of the flat sheets was reduced to 0.16 mm. Although in this initial phase reactive gas cutting with O_2 was found to not be suitable for the microcutting of AZ31, it was retained in the further study for a better comprehension of the effect of the process gas. Two conditions using the same average power at 7.5 W and pulse repetition rate at 25 kHz with O_2 and Ar as the process gas were selected for further analysis. With these selected conditions linear incisions and stent mesh were generated on the tubular material to understand better the mechanisms governing the difference in the cutting conditions with the different process gasses.

The linear incisions showed the presence of spatter around the cut kerf for both process gas conditions. However, the SEM images revealed different spatter characteristics in terms of the amount and morphology for the two cases (see Figure 4). The spatter height was estimated to be 84.6 ± 11.6 μm for the cuts made using Ar as the process gas and 26.4 ± 6.8 μm for the cuts made using O_2. A granular spatter structure with droplets around the kerf is visible on the cuts made with Ar. This observation suggests that material is ejected in the form of droplets. It can be hypothesised that explosive behaviour occurs, ejecting a portion of the material upwards, while the remaining material runs out from the lower end of the open kerf. This behaviour would be induced by ablation conditions yielding sufficiently high local temperatures to allow explosive boiling, that is, generating bubble formation, which then collapse. The splashing material is also pushed laterally with respect to the cutting direction by the process gas pressure. In contrast, the reactive cutting conditions using O_2 as the process gas show a reduced volume of spatter and an amorphous morphology, with no droplets around the cutting area. This observation suggests that the spatter was deposited from the liquid phase. Thus, the quantity of spatter generation is limited compared to the inert gas conditions. However, top-view images show an irregular and narrow kerf, suggesting that molten material is also deposited inside the kerf.

Figure 5 shows the stents cut using the different process gas conditions. The integrated machining system was able to generate the complex form of the stent, and the scrap material was kept intact on the tube. The spatter characteristics observed for the linear cuts were replicated in the production of the complicated stent mesh trajectory. Due to the increased length of the cuts, the spatter deposited in the form of droplets is more visible in the case of Ar processing. The stents cut with O_2 are overall cleaner on the surface; however, the kerf is evidently narrower. This observed narrower kerf is hypothesised to result from the formation of MgO, which possesses a high melting temperature, around the cut area. Thus, even with the increased available energy provided by the enthalpy of oxidation, kerf expansion in the lateral direction relative to the cutting front is interrupted once the MgO layer is formed.

3.2. Chemical Etching. Figure 6 reports the measured reduction values and the fitted model for the initial phase of the chemical etching study. A linear model was found to be adequate across the experimental interval. It should be noted that the regression model cannot be applied to predict thickness reduction for etching durations under 5 seconds, as the nature of the etching process changes in this regime. It can be seen that the cleaning range is limited to the first few seconds after the activation of the etching process, as half of the thickness of AZ31 sheets is removed after approximately 9 minutes of etching. An etching duration of 10 seconds was found to be the limiting duration for stent cleaning to maintain a thickness reduction no larger than 10%. This etching duration is predicted by the fitted regression model to affect a reduction of 18.8 ± 7.4 μm (95% confidence interval for the mean). However, it must be noted that the etching of tubular material in this dimension range is expected to differ from the etching of a sheet due to capillary effects inside the tube and different microstructures generated during the manufacturing processes (i.e., cold rolling for flat sheets and

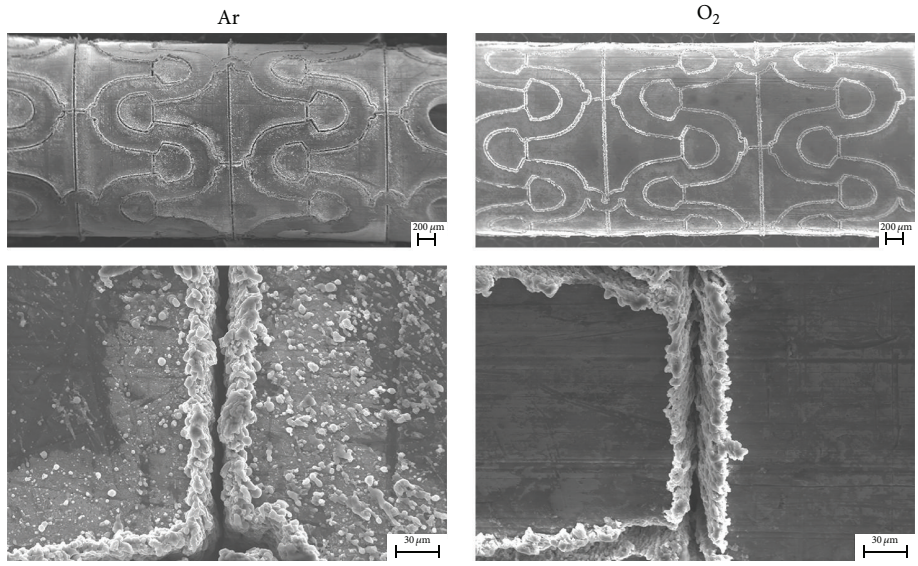

FIGURE 5: SEM images of the laser microcut stents produced using Ar and O_2.

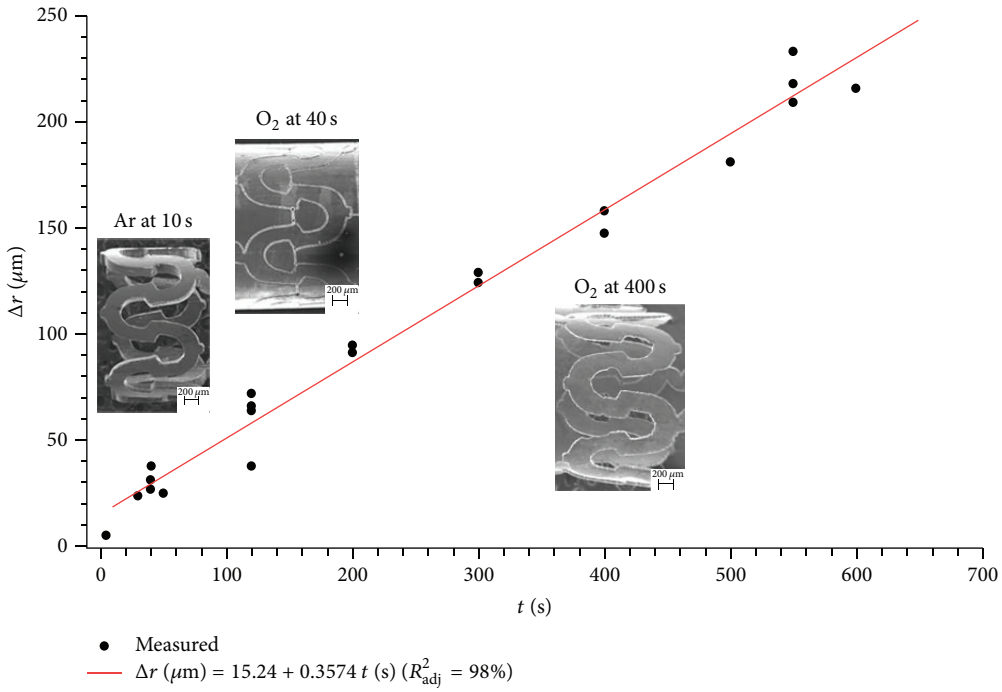

FIGURE 6: Thickness reduction of AZ31 sheets as a function of etching time, along with the etched stents from different process gas and etching conditions.

extrusion for the tubes). But the main purpose of this study is to reveal the material response to the etchant and to determine the processing range for cleaning laser microcut stent.

The stents cut with different process gas conditions, after their chemical etching, are shown in Figure 7. Although spatter on the surface was removed in both cases, the complete separation of the scrap from the stent was not possible in the case of reactive O_2 cutting, even after a prolonged etching duration of 40 seconds. This inability is due to the irregular kerf, along which loss-of-cut points can be observed. The uncut section in the deeper regions is hypothesised to be the result of interruptions caused by MgO formation, as observed also in the narrower kerf width after laser microcutting with O_2 process gas. Although chemical etching can preferentially remove the dross and oxidised zones, it does not provide complete separation at points where the process energy could not penetrate to induce cutting conditions. Further chemical etching removes the uncut sections at the same rate at which the whole stent body is reduced in thickness. Figure 8 shows

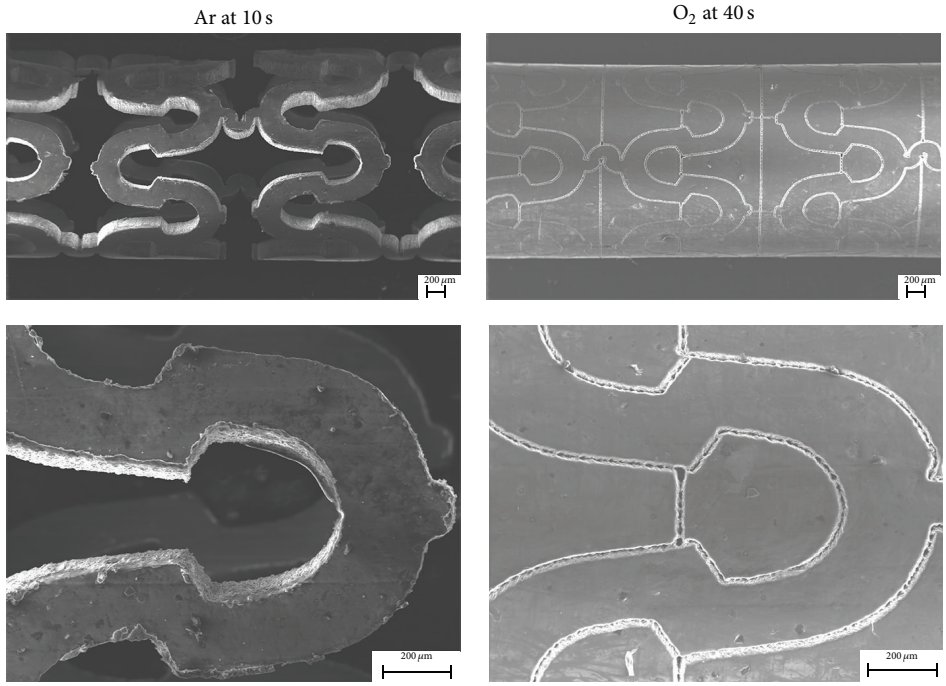

Figure 7: SEM images of the laser microcut stents using Ar and O_2, after chemical etching.

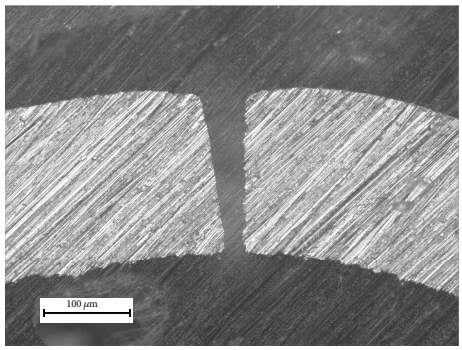

Figure 8: Cross-section of a linear incision produced using Ar as the assist gas, after chemical etching.

a cross-section of an incision made using Ar as the assist gas following its chemical etching. The cut kerf is completely clean and shows a conical form, with a kerf width of 54.8 ± 2.6 μm on top and 28.9 ± 3.8 μm on the bottom side. A cross-section of the incisions made with O_2 as the assist gas could not be obtained due to the closed kerf.

The losses of cut are observed when O_2 is used as the assist gas can be better understood by comparing the physical properties of the Mg alloy to those of the traditional stent material, stainless steel, which is commonly cut with O_2 [8, 9, 13]. Table 3 reports the physical properties of AZ31 and AISI 316L stainless steel, along with those of their main oxide components, which are MgO and FeO, respectively. In comparison to stainless steel, AZ31 has twice the oxidation enthalpy, 10 times the thermal diffusivity, and a viscosity almost 5 times lower. Although physical properties of AZ31 would appear to facilitate the generation of a higher processing energy with a more mobile molten phase, its oxide, MgO behaves as a refractory layer, preventing the processing energy from penetrating into the material. After the generation of an MgO layer inside the kerf, the primary role of O_2 is its mechanical action, pushing the generated melt out of the kerf. At this point, due to the higher melting temperature and relatively lower viscosity and thermal conductivity of MgO, the process comes to a halt locally. In the case of stainless steel, the generation of FeO does not induce such a refractory layer. Due to its low melting temperature, FeO remains in liquid form within the cut front. Furthermore, at the cutting temperatures induced (>2000 K), the Fe/FeO mixture exhibits lower viscosity than does the molten Fe (<5 mPa·s) [27]. For these reasons, complete separation of the stents cut with O_2 was only possible after longer etching: up to 400 seconds of immersion in the etchant, with excessive thickness reductions up to 160 μm (see Figure 6).

Complete separation is achievable under the inert gas cutting conditions after the previously determined 10 second chemical etching period. Using Ar as an assist gas provides shielding from excessive oxidation and also pushes the melt out of the kerf; thus, the loss of cut resulting from MgO generation is avoided. In fact, the advantages of the low melting temperature of AZ31 and the lower viscosity of Mg are exploited at these conditions, allowing a comparably low processing energy in the absence of an enthalpy of oxidation. The thickness reduction for the etched stent cut with Ar after 10 seconds of etching was measured to be 25 μm, which is slightly higher than the set limiting condition of 20 μm but within the confidence interval predicted by the regression model. In this case, the stent is free of the adhered dross on the surface, the wall quality is improved, and the edges are rounded. However, the walls require further electrochemical

Table 3: Physical properties of the biodegradable stent material AZ31, the traditional stent material AISI 316L, and the oxides of their main alloying components, MgO and FeO [27–30].

		AZ31	AISI 316L	MgO	FeO
Density	ρ (kg/m^3)	1770	8000	3580	5700
Heat capacity	c_p (J/kgK)	1020	500	920	803
Melting temperature	T_m (K)	905	1723	3098	1643
Boiling temperature	T_b (K)	1363	3273	3533	N/A
Thermal conductivity	K (W/mK)	96	21.5	50	10
Thermal diffusivity	α (m^2/s)	$5.32 \cdot 10^{-5}$	$0.54 \cdot 10^{-5}$	$1.52 \cdot 10^{-5}$	$0.22 \cdot 10^{-5}$
Oxidation enthalpy	ΔH (kJ/mol)	−602 (Mg)	−260 (Fe)	N/A	N/A
Viscosity at T_m	η (mPa s)	1.25 (Mg)	6	1.41	40

Table 4: Chemical composition of the semi-finished hollow tubes in comparison with the stents laser microcut using Ar, before and after chemical etching.

wt %	Semi-finished hollow tube	After laser microcutting with Ar		After chemical etching	
	External surface	External surface	Wall	External surface	Wall
Al	3.88	1.9 ± 0.4	1.3 ± 0.6	4.2 ± 0.8	2.1 ± 0.3
Zn	0.98	0	0	1.4 ± 0.2	0.3 ± 0.4
Mg	95.14	98.1 ± 0.4	98.7 ± 0.6	94.4 ± 0.6	97.6 ± 0.1

polishing to achieve the quality required for an implant-grade stent. This guideline has not been strictly considered in this study.

At this point, it can be concluded that the use of O_2 for the microcutting of biodegradable stents produced from AZ31 is inadequate. Thus, the final stent manufacturing process involves the use of Ar as the process gas, followed by 10 seconds of chemical etching with the ethanol HNO_3 solution.

3.3. Characterisation of the Final Stent. In Table 4, the chemical composition measurements for the final stent, produced by laser microcutting with Ar as the assist gas, are reported. Notably, most of the Al and all of the Zn are lost after laser microcutting. The complete loss of Zn within the alloy is a result of its low melting and boiling points (T_m = 693 K, T_b = 1179 K), which result in its instantaneous vaporisation during cutting. Aluminium is less prone to such vaporisation loss due to its higher boiling temperature (T_m = 933.4 K, T_b = 2767 K). The material seems to retain its chemical composition after chemical etching, as the observed values are close to the nominal composition. In the stent wall, the chemical composition differs slightly from the nominal composition due to increased thermal effects in the vicinity of the cut kerf. As a result of the thermal laser process, alloying elements are partially lost in a superficial layer, and following the removal of this layer via chemical etching, the initial alloy composition is retained.

Figure 9 presents SEM images, taken in imaging mode with back scattered electrons, of the stent after laser microcutting and after chemical etching. The darker areas in Figure 9 result from oxidised zones near the cut kerf. It is apparent that despite the fact the cutting was performed with Ar, an inert gas, surface oxidation is still present due to the high reactivity of Mg. On the other hand, after chemical etching, such zones are mostly removed.

Figure 10 reports the surface quality of the stent after laser microcutting under inert gas conditions and after chemical etching. The SEM images suggest a visible improvement in the surface roughness of the stent after chemical etching. As the spatter around the stent wall is removed, the edges are also rounded due to the polishing effect of the chemical etching. The stent roughness was R_a = 1.42 μm after the laser microcutting and R_a = 1.26 μm after the chemical etching. It is difficult to compare these roughness values with those presented in the literature because each case of material and laser source couple constitutes a completely different machining condition. However, if a comparison should be made with data available in the literature for similar cases, the measured roughness was lower than that observed for fibre laser cutting of AZ31 with a continuous wave system (R_a = 2–10 μm) [22]; slightly higher than that observed for fibre laser cutting of stainless steel with an ms-pulse system (R_a = 0.35–1 μm) [8]; similar to that observed for cutting nitinol (R_a = 1.34 μm) and higher than that observed for cutting of a platinum alloy with a ps-pulse system (R_a = 0.49 μm) [16]; and in a similar range to that observed for cutting nitinol with fs-pulse system (R_a = 0.26–2.4 μm) [17].

4. Conclusions

The present study demonstrates laser microcutting of AZ31 tubes with an ns-pulse fibre laser followed by chemical etching for biodegradable stent fabrication. The primary results obtained by this study can be summarised as follows.

(i) Laser microcutting with fibre lasers operating in the ns-regime is a feasible solution for the manufacturing of Mg alloy biodegradable stents. The advantages provided by fibre laser technology should allow further industrialisation and simplify the production of next generation stents.

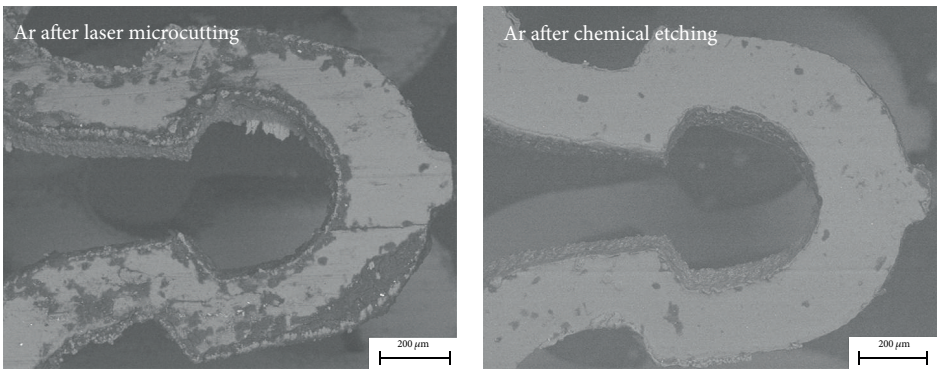

(a) (b)

Figure 9: SEM images of stents cut with Ar, taken in back scattered electron mode.

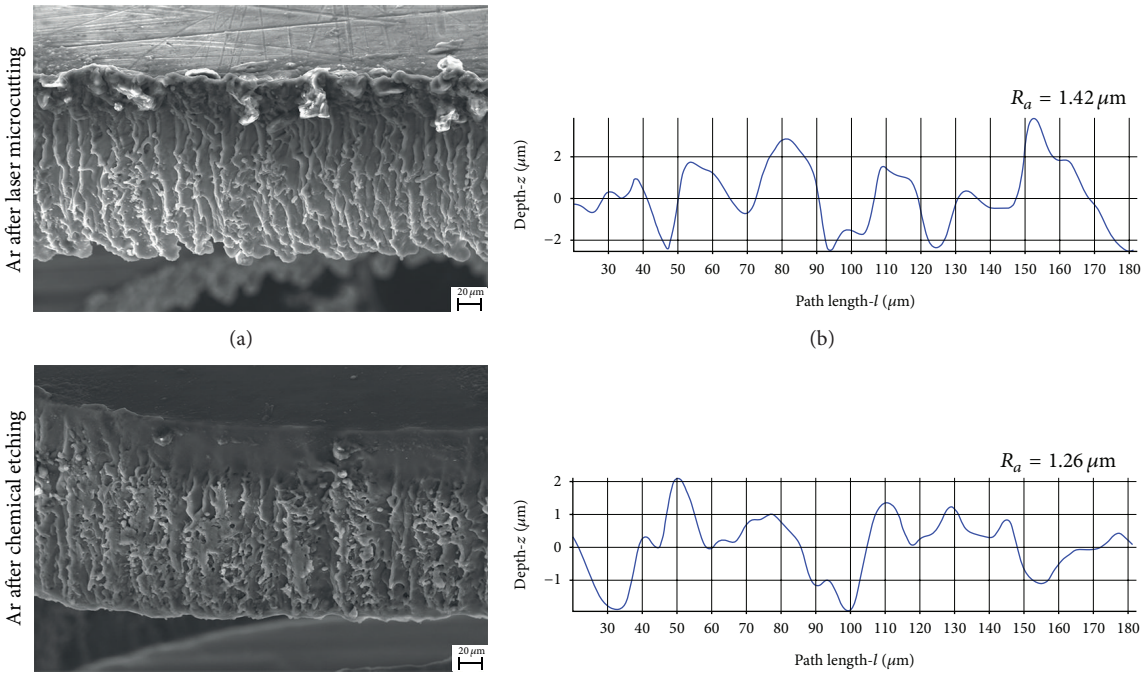

(a) (b)

(c) (d)

Figure 10: SEM images and roughness profiles of the stent after laser microcutting and chemical etching.

(ii) Laser microcutting of AZ31 Mg alloy requires inert gas conditions, rather than reactive cutting with O_2, which is the process gas used for microcutting with the traditional stent material, stainless steel. The use of O_2 results in MgO generation in the cut kerf. MgO, due to its high melting temperature, acts as a refractory layer, which precludes the cutting process from penetrating in the lateral and radial directions.

(iii) Chemical etching preferentially attacks the heat-affected and oxidised zones of laser microcut AZ31 alloy. However, thickness reduction is inevitable during the etching process. The limiting etching duration, under which thickness reduction was no more than 10% of the 200 μm thickness of the stent, was found to be 10 seconds.

(iv) Chemical etching as a finishing operation is required with laser microcutting. The applied HNO_3 ethanol solution cleaned the deposited spatter on the stent surface and cleaned the kerf in the case of stents cut with Ar. In the case of stents cut with O_2, the etchant was effective in cleaning the dross; however, kerf separation could not be completed without excessive etching durations that reduced the stent thickness to 20% of the initial thickness. After the initial removal of dross and the oxidised zone, preferential etching on the damaged zones no longer occurred and etching continued on the uncut sections of the base material as well as the stent body.

(v) The final processing path for stent manufacturing involved the use of Ar as the process gas for laser

microcutting and 10 seconds of chemical etching. Scrap parts were easily removed by chemical etching for this period of time. This etching time is shorter than a typical cleaning procedure in an isotonic bath, making this process a viable option for reducing postprocessing lead times.

(vi) The thermal laser process causes the loss of alloying compounds from the AZ31 alloy. It was possible to maintain the chemical composition of the produced stents by removing the oxidised zones with chemical etching.

(vii) The results reported here describe prototype level stents. To produce stents that are ready for implantation, electrochemical etching would be required to improve the surface quality, and surface coatings would be applied to control the biodegradation rate.

The diffusion of biodegradable and biocompatible stents in Mg alloys depends on a number of aspects that can render them competitive against the most widely used stent material, stainless steel. The control of material properties, corrosion rate, and manufacturability are the key issues, which require substantial accumulation of knowledge. Although laser microcutting of stents appears to be a widely explored field, in the case of Mg alloys, it still requires further attention. The future studies should be aimed to reveal advantages of different laser sources, not only in terms of pulse duration regime, but also in terms of different wavelengths. Although a universal laser source to fulfil all the different aspects seems still far from reality, potential solutions giving a good compromise can be identified. In this context, the ns-pulsed fibre laser sources demonstrate high flexibility, robustness, and productivity. However, the quality requirements are still challenged by the ultra-fast laser sources. Another important aspect that was not addressed in this study is the pulse shape, which is a highly influential factor on the machining quality. This factor can be the key to improve laser microcutting quality in ns-pulse regime. As a final remark, it should be noted that the use of laser beam permits more than cutting of the tubular precursor. The use of the same laser source to machine surfaces for drug insertion or biopolymer coating application, and to modify surface properties for slowing biodegradation rate, is included in the future studies.

Conflict of Interests

The authors declare that no competing and financial interests exist within the present work.

Acknowledgments

The authors would like to express their gratitude for the financial support coming from Fondazione Cassa di Risparmio di Trento e Rovereto through the project "Sviluppo di Stent Degradabili Ibridi in Magnesio con Rivestimento Polimerico per Applicazioni Biomediche" (Grant no. 2011.0250). The authors also gratefully acknowledge the experimental work carried out by Mr. Burak Kızılkaya and Mr. S. Erinç Durlanık.

References

[1] F. Witte, "The history of biodegradable magnesium implants: a review," *Acta Biomaterialia*, vol. 6, no. 5, pp. 1680–1692, 2010.

[2] M. P. Staiger, A. M. Pietak, J. Huadmai, and G. Dias, "Magnesium and its alloys as orthopedic biomaterials: a review," *Biomaterials*, vol. 27, no. 9, pp. 1728–1734, 2006.

[3] G. Mani, M. D. Feldman, D. Patel, and C. M. Agrawal, "Coronary stents: a materials perspective," *Biomaterials*, vol. 28, no. 9, pp. 1689–1710, 2007.

[4] P. Erne, M. Schier, and T. J. Resink, "The road to bioabsorbable stents: reaching clinical reality?" *CardioVascular and Interventional Radiology*, vol. 29, no. 1, pp. 11–16, 2006.

[5] R. Waksman, R. Pakala, P. K. Kuchulakanti et al., "Safety and efficacy of bioabsorbable magnesium alloy stents in porcine coronary arteries," *Catheterization and Cardiovascular Interventions*, vol. 68, no. 4, pp. 607–617, 2006.

[6] P. Zartner, R. Cesnjevar, H. Singer, and M. Weyand, "First successful implantation of a biodegradable metal stent into the left pulmonary artery of a preterm baby," *Catheterization and Cardiovascular Interventions*, vol. 66, no. 4, pp. 590–594, 2005.

[7] D. Stoeckel, C. Bonsignore, and S. Duda, "A survey of stent designs," *Minimally Invasive Therapy and Allied Technologies*, vol. 11, no. 4, pp. 137–147, 2002.

[8] A. Raval, A. Choubey, C. Engineer, and D. Kothwala, "Development and assessment of 316LVM cardiovascular stents," *Materials Science and Engineering A*, vol. 386, no. 1-2, pp. 331–343, 2004.

[9] Y. P. Kathuria, "Laser microprocessing of metallic stent for medical therapy," *Journal of Materials Processing Technology*, vol. 170, no. 3, pp. 545–550, 2005.

[10] C. Di Mario, H. Griffiths, O. Goktekin et al., "Drug-eluting bioabsorbable magnesium stent," *Journal of Interventional Cardiology*, vol. 17, no. 6, pp. 391–395, 2004.

[11] R. Erbel, C. Di Mario, J. Bartunek et al., "Temporary scaffolding of coronary arteries with bioabsorbable magnesium stents: a prospective, non-randomised multicentre trial," *The Lancet*, vol. 369, no. 9576, pp. 1869–1875, 2007.

[12] D. M. Allen, M. Simpkins, and H. Almond, "A novel photochemical machining process for magnesium aerospace and biomedical microengineering applications," *Journal of Micromechanics and Microengineering*, vol. 20, no. 10, Article ID 105010, 2010.

[13] D. M. Allen, G. Esho, and H. Almond, "Design and novel fabrication of cylindrical magnesium stents," in *Proceedings of the 1st International Conference on Design and Processes for Medical Devices*, pp. 1–6, 2012.

[14] K. F. Kleine, B. Whitney, and K. G. Wstkinds, "Use of fiber lasers for micro cutting applications in the medical device industry," in *Proceedings of the 21st International Congress on Applications of Laser and Electro-Optics (ICALEO '02)*, October 2002.

[15] H. Meng, J. Liao, Y. Zhou, and Q. Zhang, "Laser micro-processing of cardiovascular stent with fiber laser cutting system," *Optics and Laser Technology*, vol. 41, no. 3, pp. 300–302, 2009.

[16] N. Muhammad, D. Whitehead, A. Boor, and L. Li, "Comparison of dry and wet fibre laser profile cutting of thin 316L stainless steel tubes for medical device applications," *Journal of Materials Processing Technology*, vol. 210, no. 15, pp. 2261–2267, 2010.

[17] M. Mielke, D. Gaudiosi, K. Kim et al., "Ultrafast fiber laser platform for advanced materials processing," *Journal of Laser Micro Nanoengineering*, vol. 5, no. 1, pp. 53–58, 2010.

[18] N. Muhammad, D. Whitehead, A. Boor, W. Oppenlander, Z. Liu, and L. Li, "Picosecond laser micromachining of nitinol and platinum-iridium alloy for coronary stent applications," *Applied Physics A*, vol. 106, no. 3, pp. 607–617, 2012.

[19] N. Muhammad and L. Li, "Underwater femtosecond laser micromachining of thin nitinol tubes for medical coronary stent manufacture," *Applied Physics A*, vol. 107, no. 4, pp. 849–861, 2012.

[20] J. Zhu, L. Li, and Z. Liu, "CO_2 and diode laser welding of AZ31 magnesium alloy," *Applied Surface Science*, vol. 247, no. 1-4, pp. 300–306, 2005.

[21] S. M. Chowdhury, D. L. Chen, S. D. Bhole, E. Powidajko, D. C. Weckman, and Y. Zhou, "Microstructure and mechanical properties of fiber-laser-welded and diode-laser-welded AZ31 magnesium alloy," *Metallurgical and Materials Transactions A*, vol. 42, no. 7, pp. 1974–1989, 2011.

[22] L. D. Scintilla, L. Tricarico, M. Brandizzi, and A. A. Satriano, "Nd:YAG laser weldability and mechanical properties of AZ31 magnesium alloy butt joints," *Journal of Materials Processing Technology*, vol. 210, no. 15, pp. 2206–2214, 2010.

[23] T. Fushimi, M. Kitazawa, M. Endo, S. Yamaguchi, K. Nanri, and T. Fujioka, "Parametric studies on improved laser cutting performance of magnesium alloy with two flow nozzles," *Japanese Journal of Applied Physics*, vol. 43, no. 8 A, pp. 5347–5351, 2004.

[24] A. Kratky, D. Schuöcker, and G. Liedl, "Processing with kW fibre lasers—advantages and limits," in *Proceedings of the SPIE XVII International Symposium on Gas Flow, Chemical Lasers, and High-Power Lasers*, 2009.

[25] L. D. Scintilla and L. Tricarico, "Experimental investigation on fiber and CO_2 inert gas fusion cutting of AZ31 magnesium alloy sheets," *Optics & Laser Technology*, vol. 46, pp. 42–52, 2013.

[26] A. G. Demir, B. Previtali, D. Colombo et al., "Fiber laser micromachining of magnesium alloy tubes for biocompatible and biodegradable cardiovascular stents," in *Proceedings of the Fiber Lasers IX: Technology, Systems, and Applications*, January 2012.

[27] J. Powell, D. Petring, R. V. Kumar, S. O. Al-Mashikhi, A. F. H. Kaplan, and K. T. Voisey, "Laser-oxygen cutting of mild steel: the thermodynamics of the oxidation reaction," *Journal of Physics D*, vol. 42, no. 1, Article ID 015504, 2009.

[28] ASM Handbook, American Society for Metals, Metals Park, http://products.asminternational.org/hbk/index.jsp, 2013.

[29] A. Leu, S. Ma, and H. Eyring, "Properties of molten magnesium oxide," *Proceedings of the National Academy of Sciences of the United States of America*, vol. 72, no. 3, pp. 1026–1030, 1975.

[30] M. Takeda, T. Onishi, S. Nakakubo, and S. Fujimoto, "Physical properties of iron-oxide scales on Si-containing steels at high temperature," *Materials Transactions*, vol. 50, no. 9, pp. 2242–2246, 2009.

[31] W. Wu, L. Petrini, D. Gastaldi et al., "Finite element shape optimization for biodegradable magnesium alloy stents," *Annals of Biomedical Engineering*, vol. 38, no. 9, pp. 2829–2840, 2010.

[32] Q. Ge, M. Vedani, and G. Vimercati, "Extrusion of magnesium tubes for biodegradable stent precursors," *Materials and Manufacturing Processes*, vol. 27, no. 2, pp. 140–146, 2012.

[33] G. F. Vander Voort, *Metallography, Principles and Practice*, McGraw and Hill, New York, NY, USA, 1984.

[34] H. Zhao, R. Stalmans, J. Van Humbeeck, and I. De Scheerder, "Pickling of laser-cut NiTi slotted tube stents: effect on surface morphology, dimension changes and mechanical behaviour," in *Proceedings of the International Conference on Martensitic Transformations*, pp. 1125–1128, June 2002.